

ARMY RESEARCH LABORATORY



# Excitation Spectroscopy of Er<sup>3+</sup>-doped $\alpha$ -Al<sub>2</sub>O<sub>3</sub> Nanopowder and Ceramic

by T. Sanamyan, R. Pavlacka, G. Gilde, and M. Dubinskiy

ARL-TR-6126

August 2012

## **NOTICES**

### **Disclaimers**

The findings in this report are not to be construed as an official Department of the Army position unless so designated by other authorized documents.

Citation of manufacturer's or trade names does not constitute an official endorsement or approval of the use thereof.

Destroy this report when it is no longer needed. Do not return it to the originator.

# Army Research Laboratory

Adelphi, MD 20783-1197

---

---

ARL-TR-6126

August 2012

## Excitation Spectroscopy of Er<sup>3+</sup>-doped $\alpha$ -Al<sub>2</sub>O<sub>3</sub> Nanopowder and Ceramic

**T. Sanamyan and M. Dubinskiy**  
Sensors and Electron Devices Directorate, ARL

**R. Pavlacka and G. Gilde**  
Weapons and Materials Research Directorate, ARL

| REPORT DOCUMENTATION PAGE   |                             |                              | Form Approved<br>OMB No. 0704-0188                         |                                 |   |
|---|-----------------------------|------------------------------|--|---------------------------------|---|
| Public reporting burden for this collection of information is estimated to average 1 hour per response, including the time for reviewing instructions, searching existing data sources, gathering and maintaining the data needed, and completing and reviewing the collection information. Send comments regarding this burden estimate or any other aspect of this collection of information, including suggestions for reducing the burden, to Department of Defense, Washington Headquarters Services, Directorate for Information Operations and Reports (0704-0188), 1215 Jefferson Davis Highway, Suite 1204, Arlington, VA 22202-4302. Respondents should be aware that notwithstanding any other provision of law, no person shall be subject to any penalty for failing to comply with a collection of information if it does not display a currently valid OMB control number.<br><b>PLEASE DO NOT RETURN YOUR FORM TO THE ABOVE ADDRESS.</b>  |                             |                              |  |                                 |   |
| 1. REPORT DATE (DD-MM-YYYY)<br>August 2012  |                             | 2. REPORT TYPE<br>Final      |  | 3. DATES COVERED (From - To)    |   |
| 4. TITLE AND SUBTITLE<br>Excitation Spectroscopy of Er <sup>3+</sup> -doped $\alpha$ -Al <sub>2</sub> O <sub>3</sub> Nanopowder and Ceramic   |                             |                              | 5a. CONTRACT NUMBER  |                                 |   |
|   |                             |                              | 5b. GRANT NUMBER   |                                 |   |
|   |                             |                              | 5c. PROGRAM ELEMENT NUMBER                                 |                                 |   |
| 6. AUTHOR(S)<br>T. Sanamyan, R. Pavlacka, G. Gilde, and M. Dubinskiy  |                             |                              | 5d. PROJECT NUMBER   |                                 |   |
|   |                             |                              | 5e. TASK NUMBER  |                                 |   |
|   |                             |                              | 5f. WORK UNIT NUMBER                                       |                                 |   |
| 7. PERFORMING ORGANIZATION NAME(S) AND ADDRESS(ES)<br>U.S. Army Research Laboratory<br>ATTN: RDRL-SEE-M<br>2800 Powder Mill Road<br>Adelphi, MD 20783-1197  |                             |                              | 8. PERFORMING ORGANIZATION<br>REPORT NUMBER<br>ARL-TR-6126 |                                 |   |
| 9. SPONSORING/MONITORING AGENCY NAME(S) AND ADDRESS(ES)   |                             |                              | 10. SPONSOR/MONITOR'S ACRONYM(S)                           |                                 |   |
|   |                             |                              | 11. SPONSOR/MONITOR'S REPORT<br>NUMBER(S)                  |                                 |   |
| 12. DISTRIBUTION/AVAILABILITY STATEMENT<br>Approved for public release; distribution unlimited  |                             |                              |  |                                 |   |
| 13. SUPPLEMENTARY NOTES   |                             |                              |  |                                 |   |
| 14. ABSTRACT<br>We have developed an excitation spectroscopy setup for investigating the spectroscopic properties of non-transparent samples, such as powders and ceramic, in the spectral range of 380–2700 nm and temperature range of 10–300 K. We present the results of a comprehensive spectroscopic study of successfully synthesized nanopowders and fully densified transparent ceramics of erbium ion (Er <sup>3+</sup> )-doped corundum ( $\alpha$ -Al <sub>2</sub> O <sub>3</sub> ). Fluorescence and excitation spectra in a range of temperatures 10–300 K were used to infer the energy level schemes of the ground state and the first three excited Er <sup>3+</sup> multiplets ( <sup>4</sup> I <sub>15/2</sub> , <sup>4</sup> I <sub>13/2</sub> , <sup>4</sup> I <sub>11/2</sub> , and <sup>4</sup> I <sub>9/2</sub> ) in this material. The observed Er <sup>3+</sup> spectra in $\alpha$ -Al <sub>2</sub> O <sub>3</sub> nanopowders and ceramics exhibit sharp, well-resolved emission and excitation lines, indicating predominant crystalline single-site Er <sup>3+</sup> occupation. Obtained experimental data also allowed us to assess the potential of this material as the gain medium for high power laser applications in anticipation that it becomes available in a low-loss (grain-oriented) ceramic or single crystalline form in the near future. |                             |                              |  |                                 |   |
| 15. SUBJECT TERMS<br>Alumina, aluminum oxide, spectroscopy, excitation, ceramic   |                             |                              |  |                                 |   |
| 16. SECURITY CLASSIFICATION OF:   |                             |                              | 17. LIMITATION<br>OF<br>ABSTRACT<br>UU                     | 18. NUMBER<br>OF<br>PAGES<br>34 | 19a. NAME OF RESPONSIBLE PERSON<br>T. Sanamyan              |
| a. REPORT<br>Unclassified   | b. ABSTRACT<br>Unclassified | c. THIS PAGE<br>Unclassified |  |                                 | 19b. TELEPHONE NUMBER (Include area code)<br>(301) 394-2044 |

---

## Contents

---

|   |           |
|---|-----------|
| <b>List of Figures</b>                              | <b>iv</b> |
| <b>List of Tables</b>                               | <b>v</b>  |
| <b>Acknowledgments</b>                              | <b>vi</b> |
| <b>1. Introduction</b>                              | <b>1</b>  |
| <b>2. Experimental</b>                              | <b>3</b>  |
| <b>3. Results</b>                                   | <b>6</b>  |
| <b>4. Conclusions</b>                               | <b>18</b> |
| <b>5. References</b>                                | <b>20</b> |
| <b>List of Symbols, Abbreviations, and Acronyms</b> | <b>23</b> |
| <b>Distribution List</b>                            | <b>25</b> |

---

## List of Figures

---

|   |    |
|---|----|
| Figure 1. Experimental setup for excitation spectroscopy of powder and ceramic. ....  | 4  |
| Figure 2. Control interface in LabVIEW environment for the developed excitation spectroscopy of powder and ceramic. 1- spectrally and energetically corrected excitation spectrum of $\text{Er}^{3+}$ -doped $\alpha\text{-Al}_2\text{O}_3$ ; 2,3 - the raw excitation spectrum and the fluorescence signal amplitude measured from the $\alpha\text{-Al}_2\text{O}_3$ powder; 4, 5 - excitation spectrum and the signal amplitude from the reference sample (Er:YAG); 6,7 - the peak and average amplitudes of the reference pump signal, used for the energetic calibration of the excitation spectra. ....   | 5  |
| Figure 3. Room temperature fluorescence spectra from $^4\text{I}_{13/2}$ state for the two randomly chosen $\text{Er}^{3+}$ doped $\alpha\text{-Al}_2\text{O}_3$ experimental samples.....  | 7  |
| Figure 4. $\text{Er}^{3+}$ -doped $\alpha\text{-Al}_2\text{O}_3$ powder pellet and $\text{Er}^{3+}$ -doped $\alpha\text{-Al}_2\text{O}_3$ transparent ceramic presented used in the present work. ....  | 8  |
| Figure 5. Room temperature excitation spectra corresponding to the $\text{Er}^{3+} \ ^4\text{I}_{15/2} \rightarrow \ ^4\text{S}_{3/2}$ transitions at visible spectral range. ....  | 9  |
| Figure 6. Typical $\text{Er}^{3+} \ ^4\text{I}_{13/2}$ state fluorescence lifetime in $\text{Er}^{3+}$ doped $\alpha\text{-Al}_2\text{O}_3$ for three samples sintered at various temperatures. The measured values for each curve are labeled in the picture. ....   | 10 |
| Figure 7. Room temperature fluorescence spectra of $\text{Er}^{3+}$ doped powders of $\alpha\text{-Al}_2\text{O}_3$ , $\text{Y}_2\text{O}_3$ , $\text{YAlO}_3$ , and YAG. The color legend – at top right. ....   | 12 |
| Figure 8. Fluorescence spectra of $\text{Er}^{3+}$ doped $\alpha\text{-Al}_2\text{O}_3$ corresponding to the $^4\text{I}_{13/2} \rightarrow \ ^4\text{I}_{15/2}$ transition in the temperature range of 10–300 K. Shown on the insets are the blow-ups of the weak spectral features in the 1430–1500 nm (left) and 1600–1700 nm (right) spectral intervals.....  | 13 |
| Figure 9. 10-K fluorescence spectrum of $\text{Er}^{3+} \ ^4\text{I}_{13/2} \rightarrow \ ^4\text{I}_{15/2}$ transition in $\text{Er}^{3+}$ doped $\alpha\text{-Al}_2\text{O}_3$ . The arrows indicate the spectral lines corresponding to the transitions from the lowest stark sublevel of the $^4\text{I}_{13/2}$ multiplet to the lowest five sublevels of the $^4\text{I}_{15/2}$ multiplet. Indicated on the right inset (in blue) is the blow-up of the weak spectral feature in the 1620–1700 nm spectral range. Shown in red is the same spectrum averaged by using Savitzky-Golay filter. Indicated on the left inset is the energy level scheme of the $^4\text{I}_{15/2}$ ground state multiplet inferred from the spectrum. .... | 14 |
| Figure 10. Emission cross section of the $\text{Er}^{3+} \ ^4\text{I}_{13/2} \rightarrow \ ^4\text{I}_{15/2}$ transition at room (300 K) and cryogenic (77 K) temperatures in $\text{Er}^{3+}$ doped $\alpha\text{-Al}_2\text{O}_3$ . ....  | 15 |
| Figure 11. Excitation spectra corresponding to the $\text{Er}^{3+} \ ^4\text{I}_{15/2} \rightarrow \ ^4\text{I}_{13/2}$ transitions in the temperature range 10–300 K in $\text{Er}^{3+}$ doped $\alpha\text{-Al}_2\text{O}_3$ . Indicated on the inset is the energy level scheme of the $^4\text{I}_{13/2}$ multiplet inferred from these spectra.....  | 16 |
| Figure 12. Emission (from Fuchtbaer-Ladenburgh), absorption (from emission through reciprocity) and excitation cross sections for the $\text{Er}^{3+} \ ^4\text{I}_{15/2} \rightarrow \ ^4\text{I}_{13/2}$ and $^4\text{I}_{13/2} \rightarrow \ ^4\text{I}_{15/2}$ transitions at room temperature in $\text{Er}^{3+}$ doped $\alpha\text{-Al}_2\text{O}_3$ . ....  | 17 |

---

## List of Tables

---

|   |    |
|---|----|
| Table 1. Energy levels for $\text{Er}^{3+}:\alpha\text{-Al}_2\text{O}_3$ $^4\text{I}_{15/2}$ , $^4\text{I}_{13/2}$ , $^4\text{I}_{11/2}$ , $^4\text{I}_{9/2}$ manifolds in wave numbers ( $\text{cm}^{-1}$ ). Weak transitions are marked by asterisks..... | 18 |
|---|----|

---

## **Acknowledgments**

---

We gratefully acknowledge financial support of this work by the High Energy Laser Joint Technology.

---

## 1. Introduction

---

Corundum ( $\alpha$ - $\text{Al}_2\text{O}_3$ ) is the most common form of crystalline alumina (also known as sapphire). The oxygen ( $\text{O}^{2-}$ ) ions form a nearly hexagonal close-packed structure with aluminum ( $\text{Al}^{3+}$ ) ions filling two-thirds of the octahedral interstices. Each  $\text{Al}^{3+}$  center is octahedral. Corundum has a trigonal Bravais lattice with a space group of  $R\bar{3}c$  with six formula units in the hexagonal unit cell (1). Due to its unique suite of thermal, optical, and electrical properties, rare earth (RE) doped aluminum oxide (RE: $\text{Al}_2\text{O}_3$ ) is the subject of ever-growing interest as the gain material for microelectronics, integrated on-chip devices for telecommunication, and most recently, for high power laser applications. While there have been recent significant achievements in power scaling of yttrium aluminum garnet ( $\text{Y}_3\text{Al}_5\text{O}_{12}$  or YAG) based cryogenically cooled lasers with nearly diffraction limited beam quality (2), including power scaling toward laser fission application (3), the extreme pump power densities combined with the unavoidable non-radiative losses in the pump-lase process introduce severe thermally induced optical distortions in the aggressively pumped and aggressively cooled gain medium. Regardless of the sophistication of heat removal techniques and their efficiency, the insufficient thermal conductivity of the currently used gain media is the bottleneck for non-distortive heat removal. The development of innovative gain media with extremely high thermal conductivity remains the most critical technological challenge preventing power scaling of bulk high energy solid-state lasers with high beam quality.

Single crystal  $\alpha$ - $\text{Al}_2\text{O}_3$  (sapphire) has a liquid nitrogen temperature (LNT) thermal conductivity of well over 1000 W/m·K (4), which is  $\sim 40$  times higher than the LNT thermal conductivity of YAG (the most prevalent solid-state laser host) and approximately two orders of magnitude higher than the room temperature thermal conductivity of YAG. Due to the above and the favorable combination of other LNT parameters ( $dn/dT = 0.19 \times 10^{-5} \text{ K}^{-1}$ , and  $\text{CTE} = 0.34 \times 10^{-6} \text{ K}^{-1}$ ), which define the thermal figure of merit of the cryo-cooled doped  $\alpha$ - $\text{Al}_2\text{O}_3$  laser material, it can be pumped far more aggressively with far less thermally induced optical distortion. Thus, a cryo-cooled RE doped sapphire (RE:Sapphire) laser would possess extremely high power extraction capabilities, far exceeding those possessed by state-of-the-art solid-state laser gain media.

To date, RE: $\text{Al}_2\text{O}_3$  devices have been synthesized predominantly as thin films for optoelectronics applications using multiple thin-film deposition techniques. Ytterbium (Yb)-Er co-doped  $\text{Al}_2\text{O}_3$  films were prepared on silicon dioxide ( $\text{SiO}_2$ )/silicon (Si) substrate using a medium frequency magnetron sputtering system (5, 6). Erbium-doped  $\text{Al}_2\text{O}_3$  films have been deposited in a single-step process by pulsed laser deposition using independent ablation of  $\text{Al}_2\text{O}_3$  and Er targets (7). Reactive co-sputtering allows for straightforward deposition of  $\text{Er}^{3+}$  doped  $\text{Al}_2\text{O}_3$  on a variety of substrates (8). In most instances these films are *amorphous aluminum oxide* layers deposited on

Si or oxidized Si substrates aiming at applications in the future monolithic integrated optics, interconnects, and integrated optoelectronics devices in general. Amorphous RE:Al<sub>2</sub>O<sub>3</sub>, however, is not very useful for high power bulk solid-state laser applications where crystallinity is necessary to access the highest possible thermal conductivity as well acceptably high absorption and emission cross sections. The latter are largely due to the narrowband single-crystalline absorption and emission features as opposed to wideband features in amorphous materials with much lower peak cross sections.

Successful efforts in producing single-crystalline thin films of Nd<sup>3+</sup>:Al<sub>2</sub>O<sub>3</sub> grown by plasma-assisted molecular beam epitaxy (MBE) have been recently reported (9). Though MBE growth cannot be volume scaled as required for high power laser applications, these results confirmed that (1) single-crystalline sapphire *can* be doped with RE<sup>3+</sup> ions to a usable dopant level; (2) spectral features of the RE:Sapphire are, as expected, “crystalline-narrow;” (3) the spectra are consistent with single-site doping of the RE<sup>3+</sup> ion into the host crystal; and (4) RE:Sapphire exhibits sufficient peak transition cross sections, exceeding those of RE<sup>3+</sup>-doped YAG

Currently, there is no available technology to produce RE:Sapphire in the dimensions required for scalable high energy laser applications. Undoped sapphire can be grown in large sizes by a variety of melt-growth techniques. However, due to the significant ionic radius mismatch between the RE ions and the Al ion (ligand) of the host, RE elements exhibit negligible solubility within the sapphire crystal structure and tend to not incorporate into the growing crystal. Therefore, a non-traditional approach to RE:Sapphire synthesis must be adopted.

It has been demonstrated that bulk ceramics possess the capability to accommodate “less-friendly” dopants and/or significantly higher dopant levels than melt-grown crystals while maintaining sufficient optical quality for laser applications (10). This indicates that this solid-state approach allows for more “non equilibrium” dopant incorporation than traditional melt-growth techniques. In many cases (at least for cubic hosts, e.g., YAG), a highly transparent, low loss, ceramic is a suitable replacement for a single crystal for laser applications. Due to its uniaxial crystal structure, however, laser-quality transparency cannot be achieved in polycrystalline  $\alpha$ -Al<sub>2</sub>O<sub>3</sub> unless some technique of ceramic grain alignment, like magnetic grain alignment (11), is used. Additionally, the thermal conductivity of polycrystalline  $\alpha$ -Al<sub>2</sub>O<sub>3</sub> is far lower than that of sapphire. Therefore, RE-doped  $\alpha$ -Al<sub>2</sub>O<sub>3</sub> ceramics are not appropriate for high power laser gain media. On the other hand, RE-doped  $\alpha$ -Al<sub>2</sub>O<sub>3</sub> ceramics *can* potentially be used as a precursor to RE:Sapphire. One possibility is that RE-doped  $\alpha$ -Al<sub>2</sub>O<sub>3</sub> ceramics can be used as a feedstock for laser-heated pedestal growth (LHPG). Like polycrystalline ceramics, crystals grown by LHPG have been shown to be capable of “non equilibrium” dopant incorporation (12). It is possible that melting and solidification occur so rapidly in LHPG as to prevent the RE segregation that occurs during traditional melt-growth techniques. Another possibility would be to apply solid-state crystal conversion (SSCC) technique, wherein a ceramic is converted to a

single crystal via the growth of a single grain to produce RE:Sapphire. SSCC has already been used to produce large sapphire crystals (13). Crystals grown by SSCC have also been demonstrated to be capable of “non equilibrium” dopant incorporation. Therefore, the synthesis and spectroscopic characterization of RE-doped  $\alpha$ -Al<sub>2</sub>O<sub>3</sub> ceramics may enable the development of single-crystalline RE:Sapphire in dimensions and dopant concentrations adequate for high energy laser applications.

This report details the results of comprehensive spectroscopic study of Er<sup>3+</sup>-doped  $\alpha$ -Al<sub>2</sub>O<sub>3</sub> (Er:Al<sub>2</sub>O<sub>3</sub>) per our first attempt toward transparent bulk Er<sup>3+</sup>-doped sapphire gain material via ceramic route with the objective to develop a new approach to RE:Sapphire as a laser gain medium. We have achieved successful incorporation of sufficient amounts of Er<sup>3+</sup> into both highly crystalline  $\alpha$ -Al<sub>2</sub>O<sub>3</sub> powders and fully densified transparent  $\alpha$ -Al<sub>2</sub>O<sub>3</sub> ceramics. Presented here are the results of detailed spectroscopic investigation of Er<sup>3+</sup>-doped  $\alpha$ -Al<sub>2</sub>O<sub>3</sub> at all development stages. The detailed spectroscopic analysis of the ground state and the first three excited multiplets of Er<sup>3+</sup> ions in  $\alpha$ -Al<sub>2</sub>O<sub>3</sub> host are presented for the first time. These data can be successfully used for further development of high power Er<sup>3+</sup>-doped  $\alpha$ -Al<sub>2</sub>O<sub>3</sub> based lasers once the high quality Er<sup>3+</sup>-doped sapphire material is available. The processing strategies developed to (1) enhance Er<sup>3+</sup> incorporation and (2) sinter Er<sup>3+</sup>-doped  $\alpha$ -Al<sub>2</sub>O<sub>3</sub> to transparency are addressed in reference 14.

---

## 2. Experimental

---

The layout of the developed experimental setup for excitation spectroscopy of the RE doped powder and ceramic is shown in figure 1. The ACTON 2500i spectrometer was used to obtain fluorescence spectra in the spectral range of 500–1200 nm, and Nicolet 6700 Fourier transform infrared (FTIR) spectrometer was used to obtain fluorescence spectra in the wavelength range beyond 1200 nm. Both spectrometers were equipped with a standard commercial cryogenic dewar (Cryo Industries of America, Inc.), allowing temperature control and measurements in the temperature range of 10–300 K.

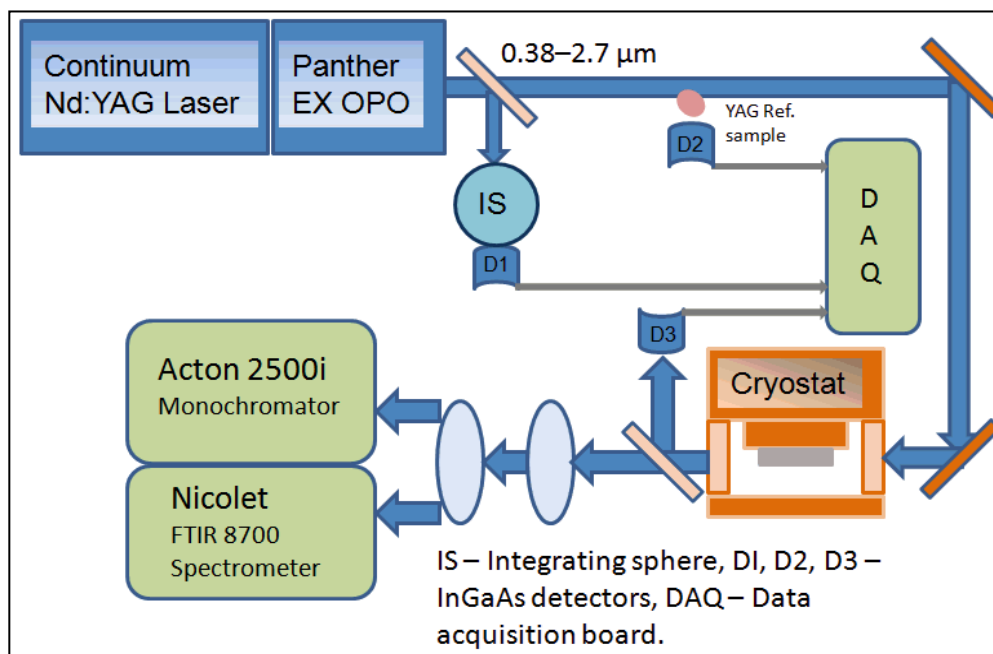


Figure 1. Experimental setup for excitation spectroscopy of powder and ceramic.

To achieve low thermal resistance of the pulverized samples (for temperature uniformity) and minimize the self-absorption effects in  $\text{Er}^{3+}$  doped  $\alpha\text{-Al}_2\text{O}_3$ , the powder samples were immersed in the thermoconductive paste and sandwiched between the two sapphire windows. The thickness of the samples used in all spectroscopic measurements was less than  $100\ \mu\text{m}$ . The sandwiched samples were attached to the copper holder and mounted on the cold finger of the cryostat. The spectral resolution of the measurement setup was better than  $1\ \text{nm}$  at room temperature and  $0.2\ \text{nm}$  at cryogenic temperatures. Excitation of  $\text{Er}^{3+}$  energy levels around  $10000\text{--}12000\ \text{cm}^{-1}$  was typically accomplished by diode lasers emitting at  $\sim 800$  and  $\sim 980\ \text{nm}$ . Occasionally, a tunable pulsed titanium (Ti)-Sapphire laser was used for fluorescence excitation at shorter wavelengths. The spectral correction of the fluorescence spectra taken with both spectrometers has been performed using a standard calibrated quartz-halogen tungsten lamp (Optronic Laboratories, LLC). The majority of samples under investigation were  $\text{Er}^{3+}$ -doped  $\alpha\text{-Al}_2\text{O}_3$  powders. Currently available sintered transparent ceramic samples were less than  $0.5\ \text{mm}$  thick; therefore, the information on  $\text{Er}^{3+}:\text{Al}_2\text{O}_3$  absorption properties was obtained using the excitation spectroscopy technique. In this case, a tunable Continuum Panther EX optical parametric oscillator (OPO) pumped by a SpectraPhysics PRO Series Laser was used as a fluorescence excitation source. The OPO was capable of delivering a few millijoules of short,  $\sim 10\text{-ns}$  pulses in the spectral range of  $400\text{--}1600\ \text{nm}$  at a  $10\text{-Hz}$  repetition rate. In order to compensate for pulse-to-pulse energy fluctuations of the excitation source, the excitation spectra were normalized to the reference signal from a photodiode, which was directly proportional to the excitation pulse energy. The overall spectral resolution of the excitation setup was limited by

the OPO output spectral width and was found to be better than  $\sim 0.3$  nm across the entire range of the excitation wavelengths. In order to double-check the validity of spectral correction, along with the  $\text{Er}^{3+}:\text{Al}_2\text{O}_3$  excitation spectra, the excitation spectra of Er:YAG, a material well known spectroscopically, excited by the same source have been collected as well (see the details in figure 1 and figure 2). The  $\text{Er}^{3+}:\text{Al}_2\text{O}_3$  lifetime measurements in the temperature range of 10–300 K were conducted by using the  $\sim 10$ -ns pulses from tunable Ti:Sapphire laser for excitation and detected by a high speed InGaAs or Si detector attached to the ACTON 2500i monochromator. The signal from the detector was processed using a TDS 2014 digital oscilloscope.

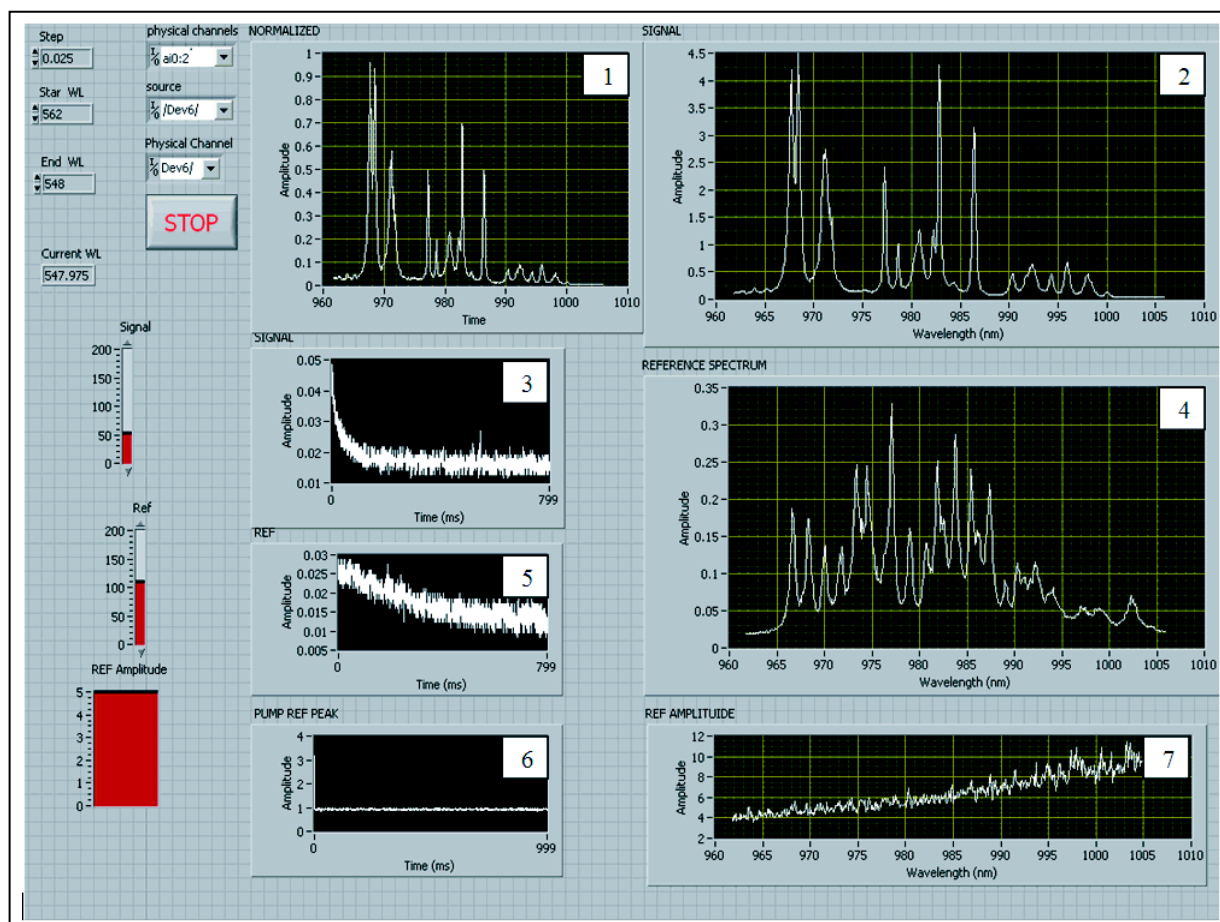


Figure 2. Control interface in LabVIEW environment for the developed excitation spectroscopy of powder and ceramic. 1- spectrally and energetically corrected excitation spectrum of  $\text{Er}^{3+}$ -doped  $\alpha\text{-Al}_2\text{O}_3$ ; 2,3 - the raw excitation spectrum and the fluorescence signal amplitude measured from the  $\alpha\text{-Al}_2\text{O}_3$  powder; 4, 5 - excitation spectrum and the signal amplitude from the reference sample (Er:YAG); 6,7 - the peak and average amplitudes of the reference pump signal, used for the energetic calibration of the excitation spectra.

Figure 2 shows the excitation spectra data acquisition control interface in the LabVIEW environment. The chart 1 in figure 2 shows the final spectrally and energetically corrected

excitation spectrum taken from the  $\text{Er}^{3+}$ -doped  $\alpha\text{-Al}_2\text{O}_3$  powder. Charts 2,3 show the raw excitation spectrum and the fluorescence signal amplitude, respectively, for the  $\alpha\text{-Al}_2\text{O}_3$  powder sample. Charts 4,5 show the excitation spectrum and signal amplitude measured for the reference signal (Er:YAG for the current measurement) and charts 6,7 show the peak and average amplitudes of the reference pump signal, used for the energetic calibration of the excitation spectra. The fluorescence spectrum in most instances was detected by a cooled InGaAs detector combined with a Stanford Research System SR 850 digital lock-in amplifier. The equipment control and data acquisition were integrated into a simple LabVIEW based program. For signal acquisition, equipment control and data processing, a NI DAQmx USB 6210 device was used in the LabVIEW environment.

Due to the fact that all spectral measurements were performed on samples that were either powders or sintered ceramics with random grain orientation, the measured fluorescence and excitation spectra were all unpolarized (polarization unresolved), though the  $\text{Er}^{3+}$ -doped  $\alpha\text{-Al}_2\text{O}_3$  is a uniaxial spectroscopic object. This merely means that all of the presented spectra can be treated as a superposition of the  $\sigma$ - and  $\pi$ - polarized spectral components.

$\text{Er}^{3+}$ -doped  $\alpha\text{-Al}_2\text{O}_3$  powder was synthesized by the co-precipitation of high purity metal nitrate and acetate solutions using a mixture of ammonium bicarbonate and ammonium hydroxide as the precipitating agent. Stoichiometry, as determined by the metal nitrate ratio prior to precipitation, was set at  $\text{Er}_{0.01}\text{Al}_{1.99}\text{O}_3$ . The amorphous precipitated powder was calcined in air and sintered in vacuum in a field-assisted sintering technology unit (FAST), which is also often referred to as spark plasma sintering (SPS). Samples were sintered at 1200 °C for 5 min. Further details of the powder synthesis and processing are addressed in reference 14.

---

### 3. Results

---

Most of the samples under investigation were  $\alpha\text{-Al}_2\text{O}_3$  powders or ceramics sintered at various temperatures, with and without co-dopants. We have implemented magnesium oxide (MgO) and/or nickel oxide (NiO) as co-dopants in order to maximize  $\text{Er}^{3+}$  doping concentration in the  $\alpha\text{-Al}_2\text{O}_3$  as well as obtain the samples with the  $\text{Er}^{3+}$  spectra indicating purely crystalline environment (with no admixture of “glassiness”) as well as nearly single-site nature of  $\text{Er}^{3+}$  activation. This resulted in an  $\text{Er}^{3+}$  doping level of 0.1–0.3 at.% in most samples. Detailed analysis of material synthesis conditions and material compositions leading to the desirable  $\text{Er}^{3+}$  spectra along with the relevant spectroscopic analysis at all development stages are presented in reference 14. All the samples obtained under optimized conditions exhibited sharp, well-resolved emission lines characteristic of  $\text{RE}^{3+}$  ions, also indicating predominant crystalline single-site  $\text{Er}^{3+}$  occupation. Typical room temperature (RT)  ${}^4\text{I}_{13/2} \rightarrow {}^4\text{I}_{15/2}$  fluorescence spectrum for three

randomly chosen experimental samples of  $\text{Er}^{3+}:\text{Al}_2\text{O}_3$  with such well-defined spectral structure is presented in figure 3. Similar spectra were previously observed in  $\text{Er}^{3+}$ -doped  $\text{Al}_2\text{O}_3$  powders prepared using the sol-gel technique (15). All experimental data presented and analyzed in this report have been obtained from  $\text{Er}^{3+}$ -doped  $\alpha\text{-Al}_2\text{O}_3$  powders and transparent ceramics with such well-defined, crystalline, highly reproducible, nearly single-site fluorescent spectra. No discernible difference was observed in spectral behavior of properly prepared powders and sintered ceramics. Single-phase nature of each and every sample was carefully monitored by x-ray diffraction (XRD) in order to confirm that we are working with phase-pure  $\alpha\text{-Al}_2\text{O}_3$ . Figure 4 displays a picture of both the  $\text{Er}^{3+}$ -doped  $\alpha\text{-Al}_2\text{O}_3$  powder pellet and  $\text{Er}^{3+}$ -doped  $\alpha\text{-Al}_2\text{O}_3$  transparent ceramic used in our spectroscopic study. The XRD measurements (14) also indicated that the powder have successfully converted to the desired alpha phase.

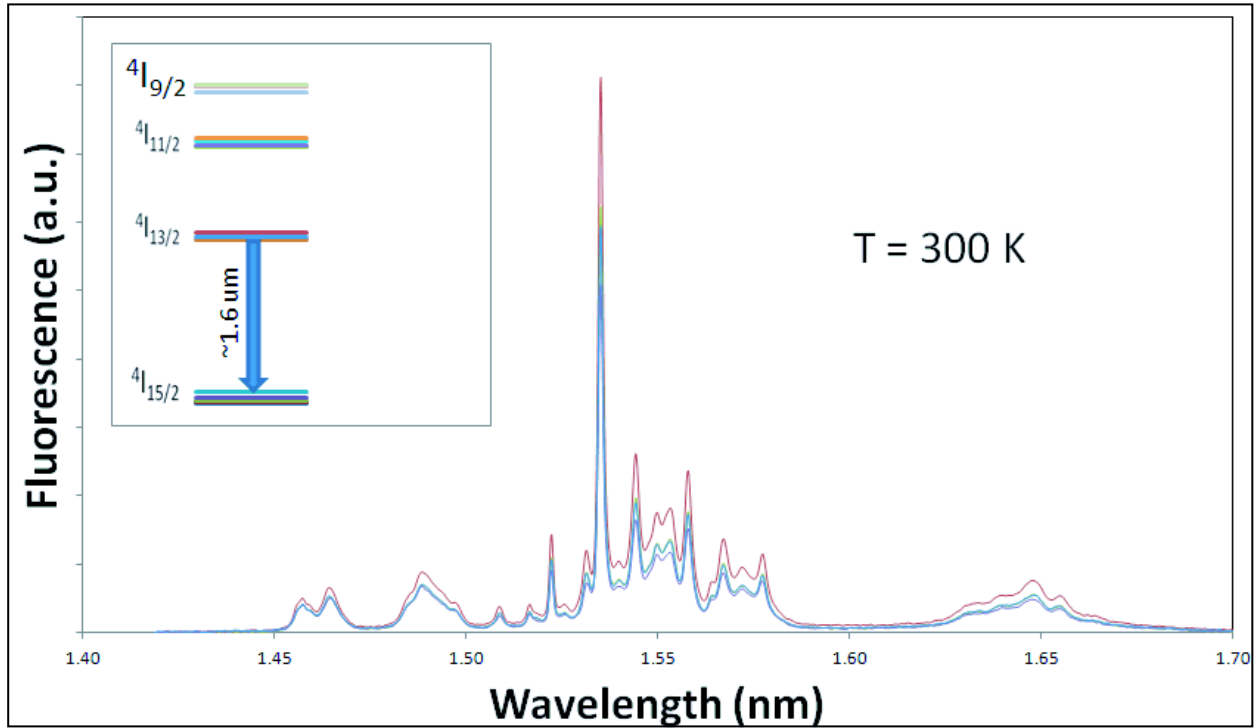


Figure 3. Room temperature fluorescence spectra from  ${}^4I_{13/2}$  state for the two randomly chosen  $\text{Er}^{3+}$  doped  $\alpha\text{-Al}_2\text{O}_3$  experimental samples.

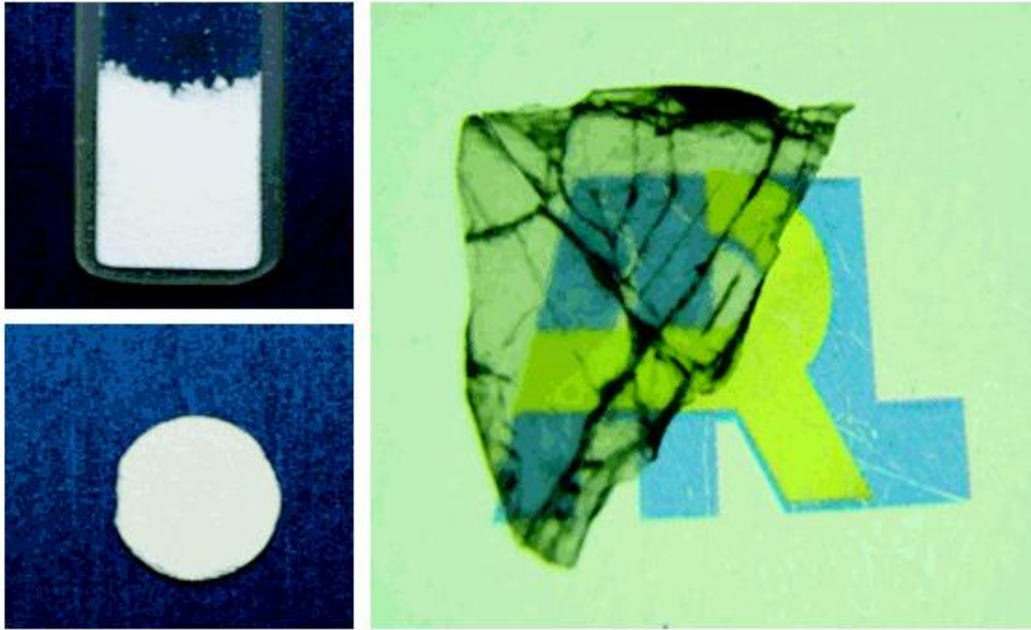


Figure 4.  $\text{Er}^{3+}$ -doped  $\alpha\text{-Al}_2\text{O}_3$  powder pellet and  $\text{Er}^{3+}$ -doped  $\alpha\text{-Al}_2\text{O}_3$  transparent ceramic presented used in the present work.

Depending on the excitation wavelength, trivalent Er ions are capable of fluorescing in a wide spectral range extending from blue to mid-IR. We have attempted to excite and observe fluorescence from all  $\text{Er}^{3+}$  levels below  ${}^2\text{H}_{11/2}$  ( $6,000\text{--}19,000\text{ cm}^{-1}$  photon energy range) by using for excitation 10-ns pulses from a tunable OPO (described earlier) in the range of  $520\text{--}1600\text{ nm}$ . We observed fluorescence from  ${}^4\text{I}_{13/2}$  manifold through excitation of  ${}^4\text{I}_{9/2}$ , as well as  ${}^4\text{F}_{9/2}$  and  ${}^4\text{S}_{3/2}$  manifolds. Figure 5 shows the excitation spectra of  ${}^4\text{S}_{3/2}$  in the vicinity of  $550\text{ nm}$  in the temperature range of  $10\text{--}100\text{ K}$ , with the details of the weak spectral transitions shown in the inset. Due to the relatively low  $\text{Er}^{3+}$  ion concentration and significant nonradiative quenching of all the states above  ${}^4\text{I}_{13/2}$ , the quality of obtained fluorescence spectra was insufficient for their detailed spectroscopic analysis. For that reason, the data presented here are based on the fluorescence measurements from the excited state with the longest lifetime,  ${}^4\text{I}_{13/2}$  ( ${}^4\text{I}_{13/2} \rightarrow {}^4\text{I}_{15/2}$  transition). Moreover, the primary interest in our investigation was the  $\text{Er } {}^4\text{I}_{13/2}$ , which are involved in Er based eye-safe laser operating at the  ${}^4\text{I}_{13/2} \rightarrow {}^4\text{I}_{15/2}$  transition. It was found that the fluorescence decay from the  ${}^4\text{I}_{13/2}$  state is single-exponential, which is consistent with the low  $\text{Er}^{3+}$  concentration, when one can assume that inter-ionic interactions between the neighboring  $\text{Er}^{3+}$  ions, as well as between the  $\text{Er}^{3+}$  ions and possible uncontrollable impurity ions are negligible. The measured lifetime values for all studied samples are found to be in the range of  $2.2\text{--}7.7\text{ ms}$ , which is consistent with the lifetime measurements of this manifold in other  $\text{Er}^{3+}$ -doped oxides (16). The large lifetime difference are because of difference of sintering temperatures of the samples. Figure 6 shows typical fluorescence decay from the  ${}^4\text{I}_{13/2}$  level of

Er<sup>3+</sup>:Al<sub>2</sub>O<sub>3</sub> for three samples, sintered at different temperatures, when excited by ~10-ns pulses at ~800 nm (excitation via the <sup>4</sup>I<sub>15/2</sub> → <sup>4</sup>I<sub>9/2</sub> absorption band). We have also investigated the temperature dependence of the <sup>4</sup>I<sub>13/2</sub> level fluorescence lifetime. In the temperature range of 10–300 K we observed only slight variations in the lifetime, which can be explained by the <sup>4</sup>I<sub>13/2</sub> population redistribution and decay from the stark sublevels <sup>4</sup>I<sub>13/2</sub> with a larger probability of spontaneous emission. Much larger values of the <sup>4</sup>I<sub>13/2</sub> → <sup>4</sup>I<sub>15/2</sub> transition peak cross sections observed at lower temperatures (shown later in figure 10) indirectly support this statement.

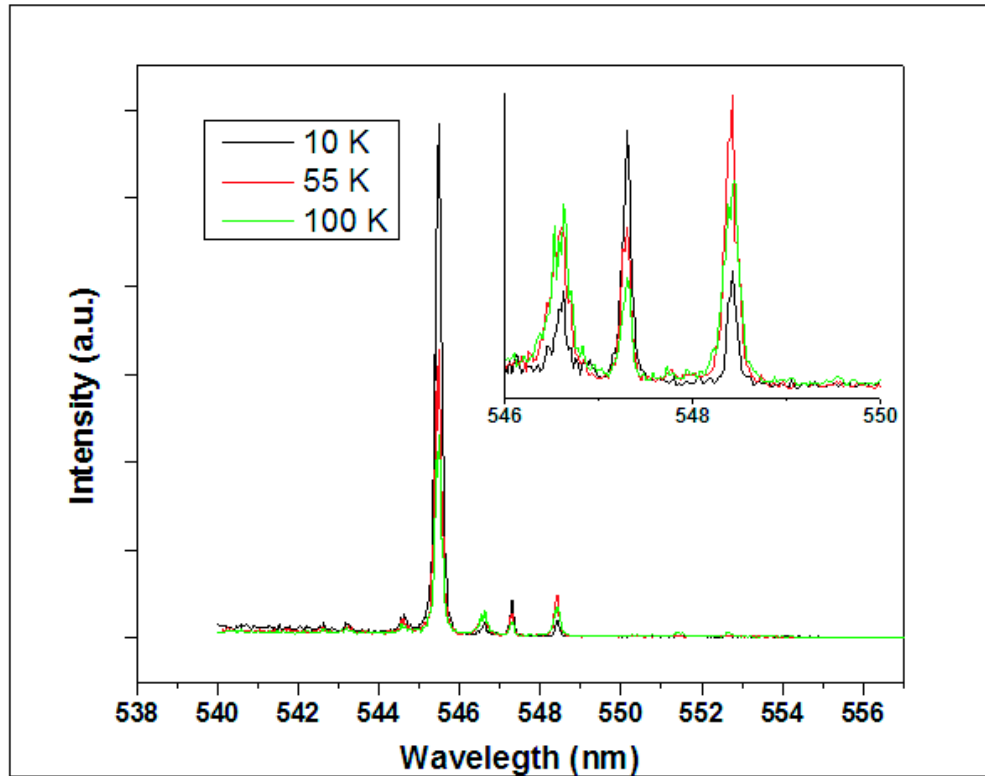


Figure 5. Room temperature excitation spectra corresponding to the Er<sup>3+</sup> <sup>4</sup>I<sub>15/2</sub> → <sup>4</sup>S<sub>3/2</sub> transitions at visible spectral range.

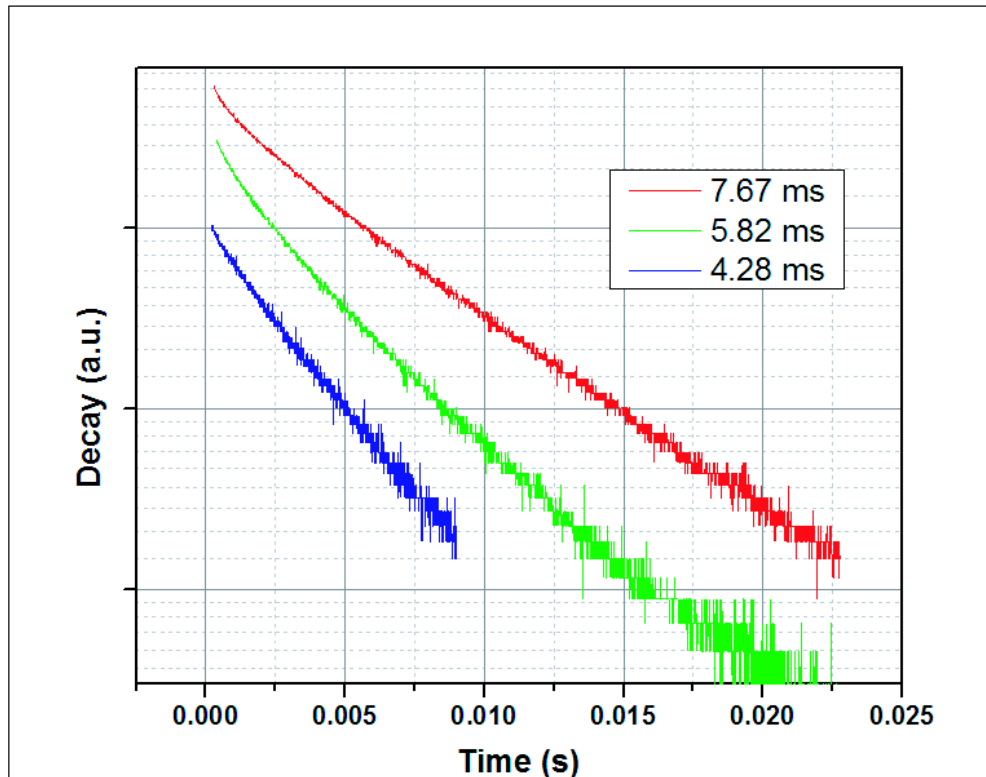


Figure 6. Typical  $\text{Er}^{3+} {}^4\text{I}_{13/2}$  state fluorescence lifetime in  $\text{Er}^{3+}$  doped  $\alpha\text{-Al}_2\text{O}_3$  for three samples sintered at various temperatures. The measured values for each curve are labeled in the picture.

The emission associated with the  ${}^4\text{I}_{13/2} \rightarrow {}^4\text{I}_{15/2}$  transition of  $\text{Er}^{3+}$  ion in  $\alpha\text{-Al}_2\text{O}_3$  is of particular practical interest since efficient, high power, eye-safe lasers based on this transition have already been successfully demonstrated in other oxide laser hosts. It was shown that these lasers can efficiently operate at relatively low  $\text{Er}^{3+}$  concentrations at both room and cryogenic temperatures (17–19). The first report on successful doping of  $\alpha\text{-Al}_2\text{O}_3$  powder with trivalent Er was presented in reference 15. Later on, the authors of reference 20 indicated that the absorption and fluorescence spectra observed in reference 15, in fact, could have originated from the residual phase of the  $\text{Er}^{3+}$ :yttrium orthoaluminate ( $\text{YAlO}_3$ ) compound. Moreover, numerous follow-on studies of Er-doped  $\text{Al}_2\text{O}_3$  have shown that the residual phases of  $\text{ErAlO}_3$ ,  $\text{ErAG}$ , and  $\text{Er}_2\text{O}_3$  compounds can be formed from starting materials as uncontrollable impurities during precipitation or calcination, and they may be responsible for the observed  $\text{Er}^{3+}$ -like fluorescence in  $\text{Al}_2\text{O}_3$  in the IR and visible spectral ranges. It is for that reason, in order to assure that the fluorescence and excitation spectra observed in this study undoubtedly originate from  $\text{Er}^{3+}$  ions in  $\alpha\text{-Al}_2\text{O}_3$ , that along with testing our own Er-doped  $\alpha\text{-Al}_2\text{O}_3$  samples we have also performed the fluorescence and excitation testing of  $\text{Er}^{3+}$ -doped YAG,  $\text{Y}_2\text{O}_3$ , and  $\text{YAlO}_3$  samples. Those samples were acquired as single crystalline and were pulverized for spectroscopic testing to

make them identical to our own samples in terms of experimental conditions. We assumed  $\text{Er}^{3+}$ -doped YAG,  $\text{Y}_2\text{O}_3$ , and  $\text{YAlO}_3$  samples to be a spectroscopic substitute for  $\text{ErAG}$ ,  $\text{Er}_2\text{O}_3$ , and  $\text{ErAlO}_3$ . It is well known that, spectroscopically,  $\text{Er}^{3+}$ -doped YAG,  $\text{Y}_2\text{O}_3$ , and  $\text{YAlO}_3$  are expected to be nearly identical or at least very similar to those of  $\text{ErAG}$ ,  $\text{Er}_2\text{O}_3$ , and  $\text{ErAlO}_3$ . Figure 7 shows the room temperature  $\text{Er}^{3+} \ ^4\text{I}_{13/2} \rightarrow \ ^4\text{I}_{15/2}$  emission spectra taken from  $\text{Er}^{3+}$ -doped  $\alpha\text{-Al}_2\text{O}_3$ , YAG,  $\text{Y}_2\text{O}_3$ , and  $\text{YAlO}_3$  powder samples. This direct comparison indicates that within the accuracy of our measurements there is no manifestation of any residual  $\text{Er}^{3+}$ -doped YAG,  $\text{Y}_2\text{O}_3$ , and  $\text{YAlO}_3$  emissions (lines) in the  $\text{Er}^{3+}$ -doped  $\alpha\text{-Al}_2\text{O}_3$  test samples used in our work. As seen from figure 7 the fluorescence spectrum of our  $\text{Er}^{3+}$ -doped  $\alpha\text{-Al}_2\text{O}_3$  powder is distinct in all of its structural details from the spectra obtained from  $\text{Er}^{3+}$ -doped YAG,  $\text{Y}_2\text{O}_3$ , and  $\text{YAlO}_3$  powders. It also has a unique single sharp emission peak at 1535.4 nm. Figure 8 shows the  $\ ^4\text{I}_{13/2} \rightarrow \ ^4\text{I}_{15/2}$  fluorescence spectra of our  $\text{Er}^{3+}$ -doped  $\alpha\text{-Al}_2\text{O}_3$  samples for a range of temperatures between 10 and 300 K. While on a relative scale, figure 8 indicates that with temperature reduction from 300 to 10 K the maximum emission cross section is going up by a factor of six. Two insets in figure 8 show the zoomed in fragments of the two relatively weak parts of fluorescence spectra in the same temperature range. The most detailed fluorescence spectrum at 10 K is shown in figure 9. It clearly exhibits the five strong spectral components at 1535.4, 1544.2, 1568.1, 1574.6, and 1578.3 nm, and the three much weaker components at 1662.2, 1665.8, and 1672.2 nm, which are zoomed in and shown on the top right inset in figure 9. The energy level diagram of the Stark-split ground state multiplet  $\ ^4\text{I}_{15/2}$  of  $\text{Er}^{3+}$  ion in  $\alpha\text{-Al}_2\text{O}_3$  inferred from the measured fluorescence spectrum at 10 K is presented on the top left inset in figure 9. For the three highest Stark levels of the energy level diagram, which were inferred from the mentioned three weakest fluorescence transitions, the energy (in  $\text{cm}^{-1}$ ) is marked by an asterisks next to it. Due to the low strength and diffuse nature of these emission lines, we could not identify these lines as related to the  $\ ^4\text{I}_{13/2} \rightarrow \ ^4\text{I}_{15/2}$  transition of  $\text{Er}^{3+}$ -doped  $\text{Al}_2\text{O}_3$  with the 100% certainty. Therefore, with the high degree of confidence, we can state that we observe five out of eight theoretically expected spectral components corresponding to the inter-Stark transitions from the lowest Stark sublevel of the  $\ ^4\text{I}_{13/2}$  multiplet to the first five lowest sublevels of the  $\ ^4\text{I}_{15/2}$  ground state multiplet. It should be noted that the energy diagram inferred from the fluorescence spectra in figure 9 substantially differs from that reported in reference 15. As mentioned in reference 20, the energy level diagram derived from the 10 K fluorescence spectra for  $\text{Er}^{3+} \ ^4\text{I}_{13/2} \rightarrow \ ^4\text{I}_{15/2}$  in reference 15 can be partially related with the fluorescence of  $\text{Er}^{3+}$  in the residual  $\text{YAlO}_3$  compound, which was likely contained in their  $\text{Er}^{3+}:\text{Al}_2\text{O}_3$  powders.

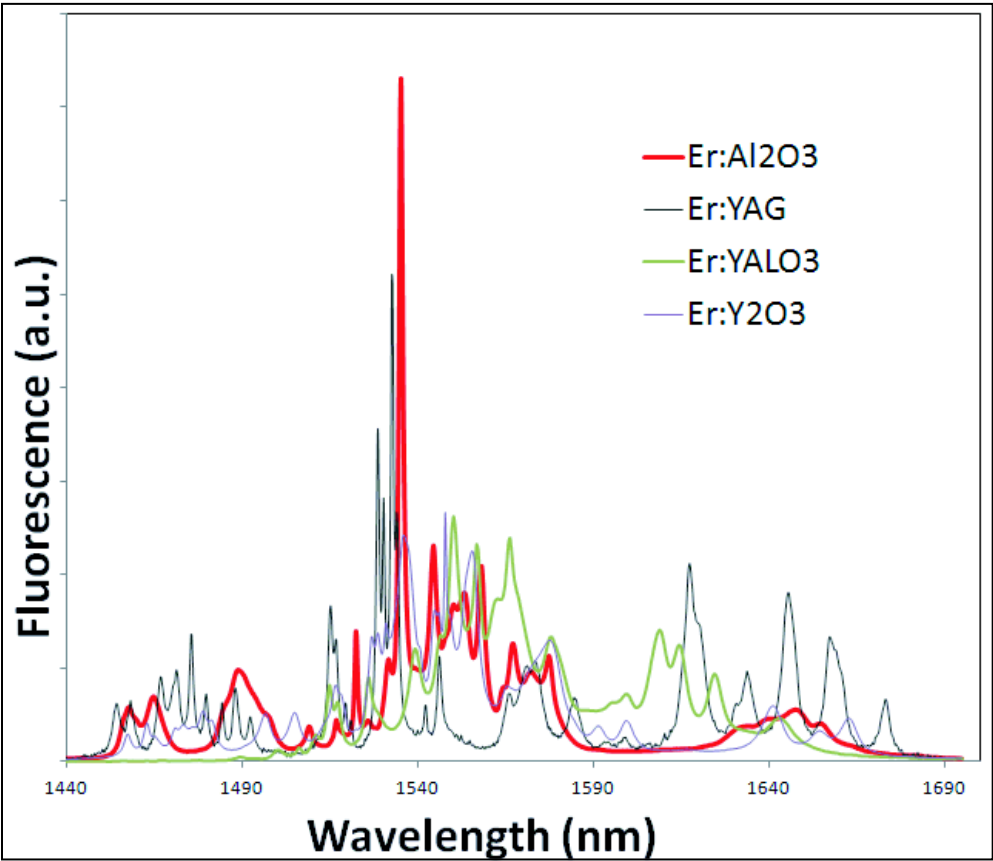


Figure 7. Room temperature fluorescence spectra of Er<sup>3+</sup> doped powders of  $\alpha$ -Al<sub>2</sub>O<sub>3</sub>, Y<sub>2</sub>O<sub>3</sub>, YAlO<sub>3</sub>, and YAG. The color legend – at top right.

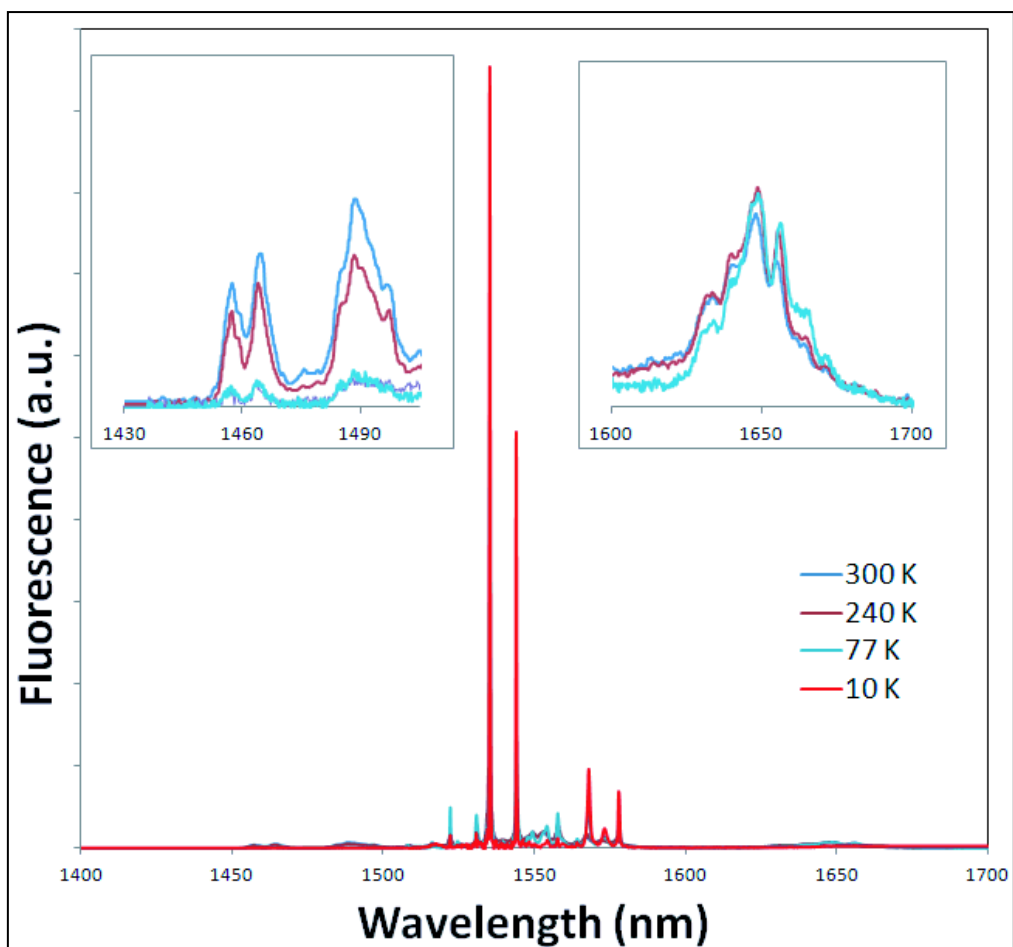


Figure 8. Fluorescence spectra of  $\text{Er}^{3+}$  doped  $\alpha\text{-Al}_2\text{O}_3$  corresponding to the  ${}^4\text{I}_{13/2} \rightarrow {}^4\text{I}_{15/2}$  transition in the temperature range of 10–300 K. Shown on the insets are the blow-ups of the weak spectral features in the 1430–1500 nm (left) and 1600–1700 nm (right) spectral intervals.

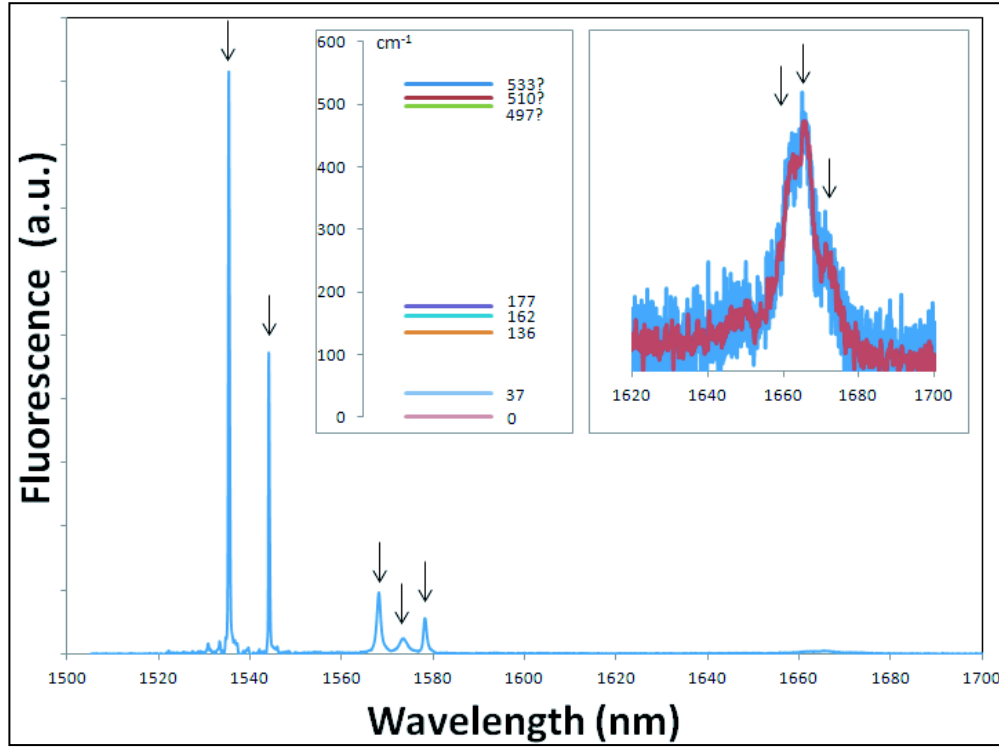


Figure 9. 10-K fluorescence spectrum of  $\text{Er}^{3+} \ ^4\text{I}_{13/2} \rightarrow \ ^4\text{I}_{15/2}$  transition in  $\text{Er}^{3+}$  doped  $\alpha\text{-Al}_2\text{O}_3$ . The arrows indicate the spectral lines corresponding to the transitions from the lowest stark sublevel of the  $\ ^4\text{I}_{13/2}$  multiplet to the lowest five sublevels of the  $\ ^4\text{I}_{15/2}$  multiplet. Indicated on the right inset (in blue) is the blow-up of the weak spectral feature in the 1620–1700 nm spectral range. Shown in red is the same spectrum averaged by using Savitzky-Golay filter. Indicated on the left inset is the energy level scheme of the  $\ ^4\text{I}_{15/2}$  ground state multiplet inferred from the spectrum.

From the measured fluorescence spectrum and the radiative lifetime,  $\tau$  of the  $\ ^4\text{I}_{13/2}$  multiplet one can derive the stimulated emission cross section using the well-known Fuchtbauer-Ladenburg method (21):

$$\sigma_{emi} = \frac{\eta \lambda^5}{8\pi n^2 c \tau \int \lambda I(\lambda) d\lambda} \quad (1)$$

where  $\sigma_{emi}$  is the emission cross section,  $\eta$  is the fluorescence quantum efficiency,  $\lambda$  is the fluorescence wavelength, and  $n$  and  $c$  are the refractive index and the light velocity, respectively. It should be noted that for the cross section derivation the longest measured lifetime, 7.7 ms, was used. This is based on an assumption that in the samples exhibiting the longest fluorescence lifetime the nonradiative quenching processes are negligible and, thus, the observed  $\ ^4\text{I}_{13/2} \rightarrow \ ^4\text{I}_{15/2}$  transition lifetime is purely radiative. For the same reason, with this longest lifetime chosen for an estimate, the quantum efficiency  $\eta$  of this transition is assumed to be close to 1. The emission cross section spectrum of the  $\ ^4\text{I}_{13/2} \rightarrow \ ^4\text{I}_{15/2}$  transition obtained from the above derivation is presented in figure 10 for both RT and LNT. It can be seen that  $\text{Er}^{3+}$  ion in  $\alpha\text{-Al}_2\text{O}_3$  host has the

cross section values quite adequate for an efficient laser. It should be suitable for high power laser operation based on the  ${}^4I_{13/2} \rightarrow {}^4I_{15/2}$  transition. The highest laser power scaling potential is expected at cryogenic temperatures where the observed peak cross section is practically on par with that of RT  $\text{Nd}^{3+}$ -doped YAG. The excitation spectra corresponding to the  ${}^4I_{15/2} \rightarrow {}^4I_{13/2}$  inter-multiplet transitions are shown in figure 11. Similarly to what was observed in the fluorescence spectra, we found four strong excitation lines at 1509.4, 1516.1, 1522.3, and 1535.4 nm and three much weaker components at 1455.8, 1457.1, and 1459.0 nm, shown on the top left inset of figure 11. The inferred energy level diagram of the  ${}^4I_{13/2}$  multiplet is shown on a second inset. For the reasons mentioned earlier in relevance to the  ${}^4I_{13/2} \rightarrow {}^4I_{15/2}$  fluorescence spectra, for these weak transitions, the corresponding energy levels on the diagram have an asterisk next to the level energy.

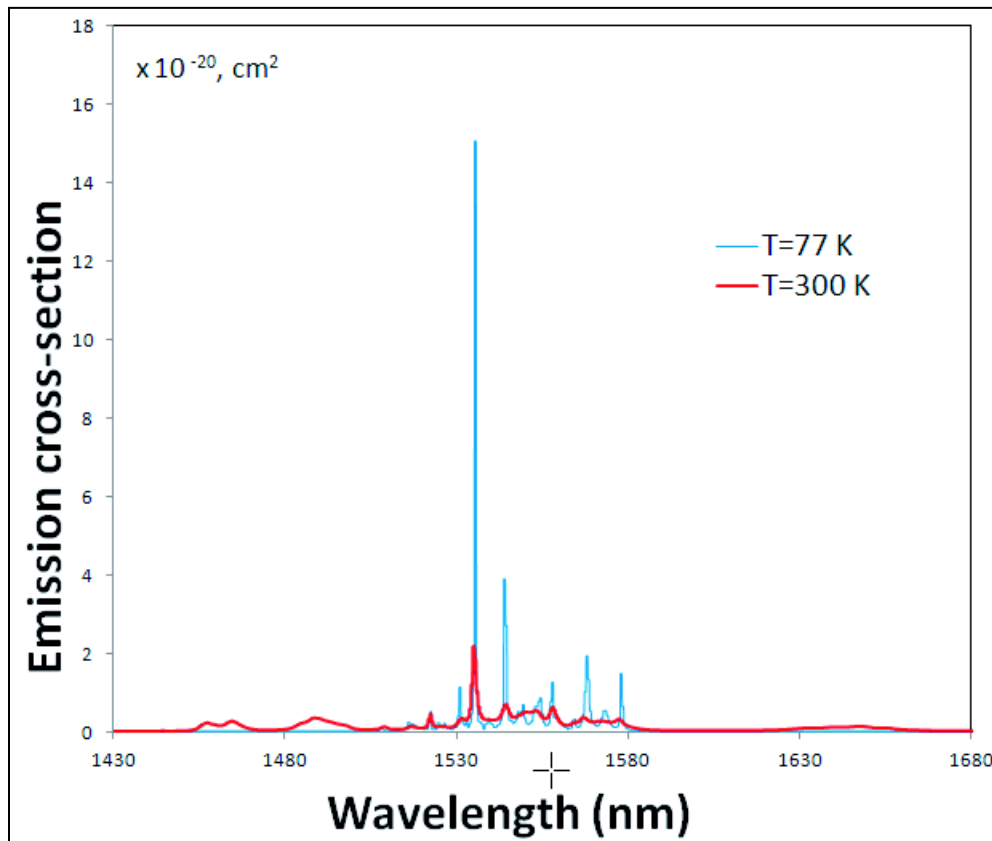


Figure 10. Emission cross section of the  $\text{Er}^{3+} {}^4I_{13/2} \rightarrow {}^4I_{15/2}$  transition at room (300 K) and cryogenic (77 K) temperatures in  $\text{Er}^{3+}$  doped  $\alpha\text{-Al}_2\text{O}_3$ .

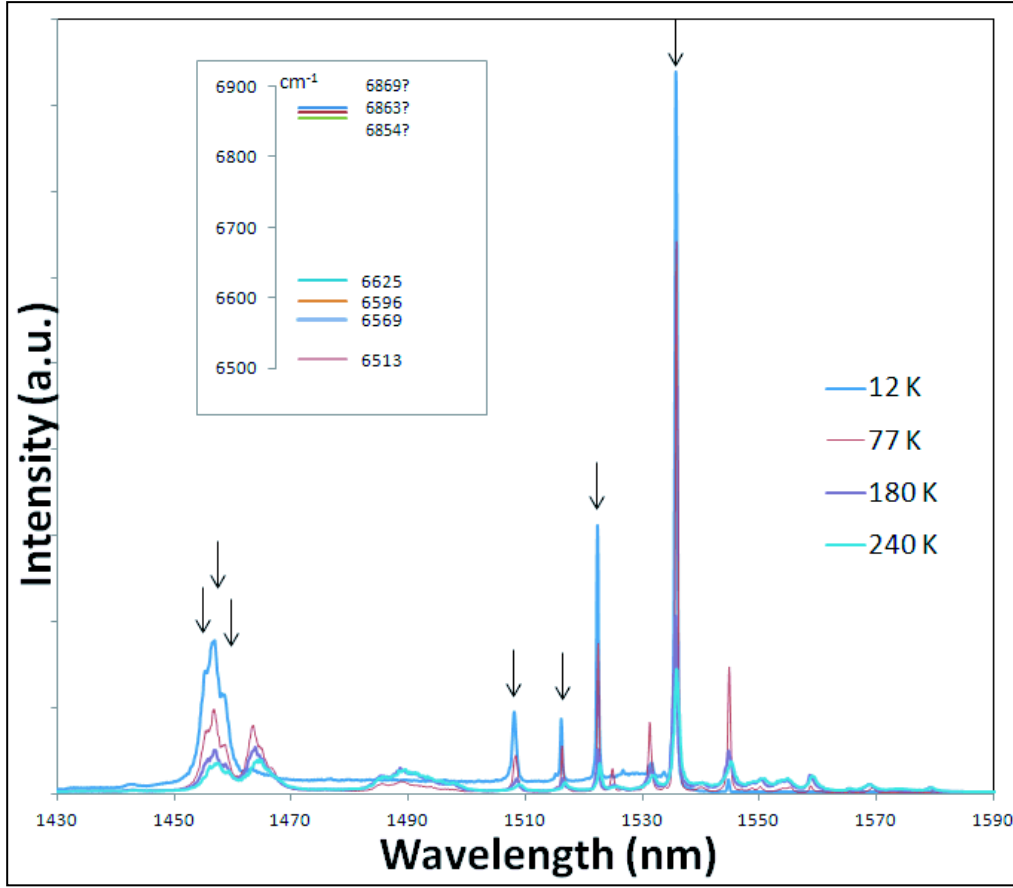


Figure 11. Excitation spectra corresponding to the  $\text{Er}^{3+} \ ^4\text{I}_{15/2} \rightarrow \ ^4\text{I}_{13/2}$  transitions in the temperature range 10–300 K in  $\text{Er}^{3+}$  doped  $\alpha\text{-Al}_2\text{O}_3$ . Indicated on the inset is the energy level scheme of the  $\ ^4\text{I}_{13/2}$  multiplet inferred from these spectra.

Because at the moment we do not have any transparent samples suitable for direct absorption measurements, it behooves us to compare the obtained excitation spectra for the  $\ ^4\text{I}_{15/2} \rightarrow \ ^4\text{I}_{13/2}$  transition with the absorption cross section for the same transition. The absorption cross section can be inferred from the Fuchtbauer-Ladenburg derived emission cross section by reciprocity from the following well-known expression (22):

$$\sigma_{abs} = \sigma_{emi} \frac{Z_U}{Z_L} \exp\left(\frac{\frac{hc}{\lambda} - E_{ZL}}{kT}\right) \quad (2)$$

where  $\sigma_{abs}$  and  $\sigma_{emi}$  are absorption and emission cross sections;  $Z_U$  and  $Z_L$  are partition functions for the upper  $\ ^4\text{I}_{13/2}$  and the lower  $\ ^4\text{I}_{15/2}$  states;  $E_{ZL}$  is the zero line photon energy, i.e., the energy separation between the lowest stark sublevels of the  $\ ^4\text{I}_{13/2}$  and  $\ ^4\text{I}_{15/2}$  multiplets;  $k$ ,  $c$ , and  $\lambda$  are the Planck constant, light velocity, and transition wavelength, respectively; and  $T$  is the temperature of the host. The calculation results are presented in figure 12. As can be seen from figure 12,

there is a satisfactory agreement between the relative excitation peak strength and the absorption cross sections.

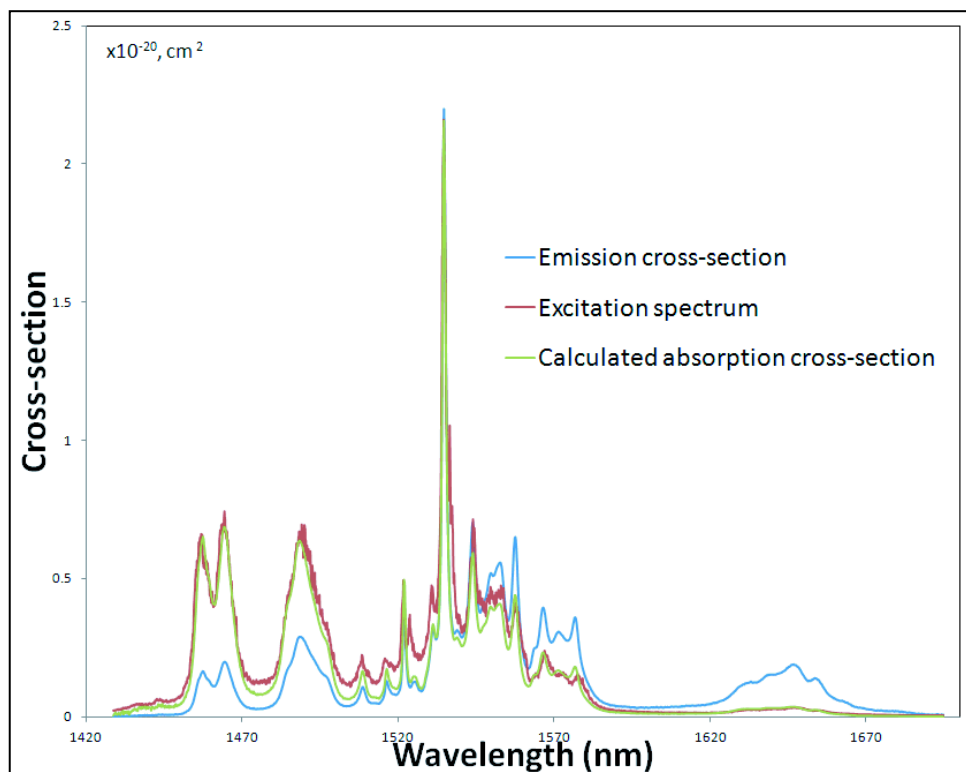


Figure 12. Emission (from Fuchtbaer-Ladenburgh), absorption (from emission through reciprocity) and excitation cross sections for the  $\text{Er}^{3+} {}^4\text{I}_{15/2} \rightarrow {}^4\text{I}_{13/2}$  and  ${}^4\text{I}_{13/2} \rightarrow {}^4\text{I}_{15/2}$  transitions at room temperature in  $\text{Er}^{3+}$  doped  $\alpha\text{-Al}_2\text{O}_3$ .

The energy structure of the  ${}^4\text{I}_{1/2}$  manifold is also of great practical importance since most of Er-based solid-state lasers are currently pumped through this level. This manifold provides sufficiently strong absorption in the spectral range of emission of commercially available InGaAs/AlGaAs) 980-nm semiconductor lasers. Moreover, this level in most oxide laser materials is metastable, with the lifetime varying from the shortest ( $\sim 0.1$  ms) in Er:YAG to the longest ( $\sim 3.6$  ms) in Er: yttrium oxide ( $\text{Y}_2\text{O}_3$ ) (23). Lasers emitting around  $\sim 3$   $\mu\text{m}$  have been built based on a number of  $\text{Er}^{3+}$ -doped oxide hosts (Er:YAG, Er:YAlO<sub>3</sub> Er:Y<sub>2</sub>O<sub>3</sub>, etc.), where laser action is initiated from this level, and exploits the nominally self-terminated  ${}^4\text{I}_{1/2} \rightarrow {}^4\text{I}_{13/2}$  laser transition (24). The fluorescence from this level in our  $\text{Er}^{3+}$ -doped  $\text{Al}_2\text{O}_3$  samples was too weak in order to be used for any sensible interpretation. The high multiphonon decay rate of the  ${}^4\text{I}_{1/2}$  level in this material is due to the fact that the energy gap between this and the next level down ( ${}^4\text{I}_{13/2}$ ) is only about  $3000\text{ cm}^{-1}$  and the maximum phonon frequency of this host material is  $\sim 750\text{ cm}^{-1}$  (one of the highest among the oxide laser hosts) (25). The excitation spectrum taken at 10 K corresponds to the transitions from the lowest Stark sublevel of the ground state multiplet

$^4I_{15/2}$  to all Stark sublevels of the  $^4I_{11/2}$  state. At this temperature, we observed five out of six (expected theoretically) spectral components at 964.2, 965.0, 973.8, 975.2, and 979.5 nm. The Stark sublevels energy positions, inferred from the 10-K excitation spectra are shown in table 1. A very weak spectral component at  $10322\text{ cm}^{-1}$ , marked in the table by an asterisk, which can only be discerned after thorough data analysis and noise filtering in the 967–969 nm spectral range can actually be interpreted as a missing line of the  $^4I_{15/2} \rightarrow ^4I_{11/2}$  transition at 968.8 nm.

Table 1. Energy levels for  $\text{Er}^{3+}:\alpha\text{-Al}_2\text{O}_3$   $^4I_{15/2}$ ,  $^4I_{13/2}$ ,  $^4I_{11/2}$ ,  $^4I_{9/2}$  manifolds in wave numbers ( $\text{cm}^{-1}$ ). Weak transitions are marked by asterisks.

| $^4I_{15/2}$ | $^4I_{13/2}$ | $^4I_{11/2}$ | $^4I_{9/2}$ |
|--------------|--------------|--------------|-------------|
| 0            | 6513         | 10209        | 12365       |
| 37           | 6569         | 10254        | 12376       |
| 136          | 6596         | 10269        | 12595       |
| 162          | 6625         | 10322*       | 12618       |
| 177          | 6854*        | 10363        | 12631       |
| 497*         | 6863*        | 10371        |             |
| 510*         | 6869*        |              |             |
| 533*         |              |              |             |

Normally, fluorescence from the  $^4I_{9/2}$  level of  $\text{Er}^{3+}$  ion is quenched by severe multiphonon relaxation (in almost all oxides) and only in a few hosts (the so-called low-phonon hosts) is it observable. The fluorescence signal from this level in  $\text{Er}^{3+}$ -doped  $\text{Al}_2\text{O}_3$  was also too weak to be used for any meaningful interpretation. Nevertheless, we have extensively explored the excitation spectra corresponding to the  $^4I_{15/2} \rightarrow ^4I_{9/2}$  transition in a wide temperature range. Knowledge of the energy level diagram of this level is also important since the  $^4I_{15/2} \rightarrow ^4I_{9/2}$  absorption band of  $\text{Er}^{3+}$  is very suitable for pumping with another efficient commercially available InGaAs/AlGaAs semiconductor lasers emitting around 800 nm. We have observed all five absorption lines (expected theoretically) in the 10-K excitation spectrum. The energy level positions for the  $^4I_{9/2}$  state corresponding to the spectral range 788–823 nm, derived from the 10-K excitation spectrum are shown in table 1. The absorption peaks at 791.7, 792.5, 793.9, 808, and 808.7 nm are identified as corresponding to the  $^4I_{15/2} \rightarrow ^4I_{9/2}$  inter-multiplet transitions.

---

## 4. Conclusions

---

This work presents spectroscopic evidence that the trivalent Er ions can be successfully doped into  $\alpha\text{-Al}_2\text{O}_3$  host despite the significant ionic radius mismatch between the dopant and ligand. The observed  $\text{Er}^{3+}$  ion spectra in  $\alpha\text{-Al}_2\text{O}_3$  nanopowders and fully densified ceramics are a manifestation of purely crystalline environment and also indicate the nearly single-site nature of  $\text{Er}^{3+}$  activation. So far we achieved  $\text{Er}^{3+}$  doping level of 0.1–0.3 at.% in most of our samples. The emission cross section (derived via Fuchtbauer-Ladenburg routine) followed by absorption cross

section derived from reciprocity are presented for both room and cryogenic temperatures. Presented detailed spectroscopic study of the ground state ( $^4I_{15/2}$ ) and the first three excited  $Er^{3+}$  multiplets ( $^4I_{13/2}$ ,  $^4I_{11/2}$ , and  $^4I_{9/2}$ ) in this material can be successfully used for future design and development of high power Er:Sapphire based lasers. The currently planned crystal field calculations for  $Er^{3+}$  ion in an octahedral  $Al^{3+}$  position will answer the question of whether the observed spectral behavior supports the hypothesis of  $Er^{3+}$  ion incorporation into  $Al^{3+}$  site in  $\alpha$ - $Al_2O_3$  single crystal structure.

---

## 5. References

---

1. Newnham, R. E.; de Haan, Y. M. Refinement of the  $\alpha$ -Al<sub>2</sub>O<sub>3</sub>, Ti<sub>2</sub>O<sub>3</sub>, V<sub>2</sub>O<sub>3</sub> and Cr<sub>2</sub>O<sub>3</sub> Structures. *Zeitschrift für Kristallographie* **1962**, *117* (2–3), 235–237.
2. Fan, Tso Yee; Ripin, Daniel J.; Aggarwal, Roshan L.; Ochoa, Juan R.; Chann, Bien; Tilleman, Michael; Spitzberg, Joshua. Cryogenic Yb<sup>3+</sup>-doped Solid-state Lasers. *IEEE J. Sel. Topics Quantum Electron.* **2007**, *13* (3), 448–459.
3. Tokita, S.; Kawanaka, J.; Fujita, M.; Kawashima, T.; Izawa, Y. Sapphire-conductive End-cooling of High Power Cryogenic Yb:YAG Lasers. *Appl. Phys. B* **2005**, *80* (6), 635–638.
4. Holland, M. G. Thermal Conductivity of Several Optical Maser Materials. *J. Appl. Phys.* **1962**, *33* (9), 2910–2911.
5. Cattaruzza E.; Back, M.; Battaglin G.; Riello, P.; Trave, E. Er-doped Alumina Crystalline Films Deposited by Radiofrequency Magnetron Co-sputtering. *Opt. Mater.* **2011**, *33* (7), 1135–1138.
6. Song, Q.; Li, C.; Li, J.; Ding, W.; Xu, J.; Deng, X.; Song, C. Photoluminescence Properties of the Yb : Er Co-doped Al<sub>2</sub>O<sub>3</sub> Thin Film Fabricated by Microwave ECR Plasma Source Enhanced RF Magnetron Sputtering. *Opt. Mater.* **2006**, *28* (12), 1344–1349.
7. Serna, R.; Nunez-Sanchez, S.; Xu, Fei.; Afonso, C. N. Enhanced Photoluminescence of Rare-earth Doped Films Prepared by Off-axis Pulsed Laser Deposition. *Appl. Surf. Sci.* **2011**, *257*, 5204–5207.
8. Agazzi, Laura; Bradley, Jonathan D. B.; Dijkstra, Meindert; Ay, Feridun; Roelkens, Gunther; Baets, Roel; Wörhoff, Kerstin; Pollnau, Markus. Monolithic Integration of Erbium-doped Amplifiers with Silicon-on-insulator Waveguides. *Optics Express* **2010**, *18* (26), 27703–27711.
9. Kumaran, R.; Tiedje, T.; Webster, S. E.; Penson, S.; Li, Wei. Epitaxial Nd-doped  $\alpha$ -(Al<sub>1-x</sub>Ga<sub>x</sub>)<sub>2</sub>O<sub>3</sub> Films on Sapphire for Solid-state Waveguide Lasers. *Opt. Lett.* **2012**, *35* (22), 3793–3795. (or In Ref).
10. Ikesue, A.; Aung, Y. L.; Taira, T.; Kamimura, T.; Yoshida, K.; Messing, G. L. Progress in Ceramic Lasers. *Annual Review of Materials Research* **2006**, *36*, 397–429.
11. Taira, T. Domain-Controlled Laser Ceramics toward Giant Micro-Photonics. *Opt. Mat. Express* **2011**, *1* (5), 1040–050.

12. Krebs, J. K.; Happek, U. Yb<sup>3+</sup> Energy Levels in  $\alpha$ -Al<sub>2</sub>O<sub>3</sub>. *J. Lumin.* **2001**, 94–95, 65–68.
13. Scott, C.; Kaliszewski, M.; Greskovich, C.; Levinson, L. Conversion of Polycrystalline Al<sub>2</sub>O<sub>3</sub> into Single-Crystal Sapphire by Abnormal Grain Growth. *J. American Ceramic Society* **2002**, 85 (5) 1275–1280.
14. Pavlacka, R.; Sanamyan, T.; Gilde, G.; Dubinskiy, M. Synthesis and Characterization of Er Doped Al<sub>2</sub>O<sub>3</sub>. submitted to Optical Materials.
15. Kaplyanskii, A. A.; Kulinkin, A. B.; Kutsenko, A. B.; feofilov, S. P.; Zakharchenya, R. I.; Vasilevskaya, T. N. Optical Spectra of Triply-charged Rare-earth Ions in Polycrystalline Corundum. *Phys. Solid State* **1998**, 40 (8), 1310–1316.
16. Ter-Gabrielyan, N.; Dubinskiy, M.; Newburgh, G.; Michael, A.; Merkle, L. Temperature Dependence of a Diode-Pumped Cryogenic Er:YAG Laser. *Opt. Express* **2009**, 17 (9), 7158–7169.
17. Ter-Gabrielyan, N.; Fromzel, V.; Dubinskiy, M. Performance Analysis of the Ultra-low Quantum Defect Er<sup>3+</sup>:Sc<sub>2</sub>O<sub>3</sub> Laser. (*Invited paper*) - *Opt. Mater. Express* **2011**, 1 (3), 503–513.
18. Ter-Gabrielyan, N.; Merkle, L. D.; Newburgh, G. A.; Dubinskii, M. Resonantly-pumped Er<sup>3+</sup>:Y<sub>2</sub>O<sub>3</sub> Ceramic Laser for Remote CO<sub>2</sub> Monitoring. *Laser Physics* **2009**, 19, 867–869.
19. Ter-Gabrielyan, N.; Merkle, L. D.; Ikesue, A.; Dubinskii, M. Ultra-Low Quantum Defect Eye-safe Er:Sc<sub>2</sub>O<sub>3</sub> Laser. *Optics Letters* **2008**, 33, 1524–1526.
20. Tanner, P.A.; Wong, K. L.; Liang, Y. Multiple Phase Production of Doping Er<sup>3+</sup> Into  $\alpha$ -Al<sub>2</sub>O<sub>3</sub>. *Chem. Phys. Lett.* **2004**, 399 (1–3), 15–19.
21. Aull, Brian F.; Jenssen, Hans P. Vibronic Interactions in Nd:YAG Resulting in Nonreciprocity of Absorption and Stimulated Emission Cross Sections. *IEEE J. Quantum Electron.* QE-18(5), 925–929 (1982).
22. Payne, S. A.; Chase, L. L.; Smith, L. K.; Kway, W. L.; Krupke, W. F. Infrared Cross Section Measurements for Crystals Doped with Er<sup>3+</sup>, Tu<sup>3+</sup> and Ho<sup>3+</sup>. *IEEE J. Quantum Electron.* **1992**, 28 (11), 2619–2629.

23. Sanamyan, T.; Simmons, J.; Dubinskii, M. Efficient Cryo-cooled 2.7- $\mu\text{m}$  Er<sup>3+</sup>:Y<sub>2</sub>O<sub>3</sub> Ceramic Laser with Direct Diode Pumping of the Upper Laser. *Phys. Lett.* **2010**, 7 (8), 569–572.
24. Zhekov, V. I.; Lobachev, V. A.; Murina, T. M.; Prokhorov, A. M. Efficient Cross-relaxation Laser Emitting at = 2.94  $\mu\text{m}$ . *Sov. J. Quantum Electron.* **1983**, 13 (9), 1235–1237.
25. Porto, S.P.S.; Krishnan, R. S. Raman Effect of Corundum. *J. Chem Phys.* **1967**, 47 (3), 1009–1012.

---

## List of Symbols, Abbreviations, and Acronyms

---

|  |  |
|--|--|
| Al                                       | aluminum   |
| AlGaAs                                   | aluminum gallium arsenide                          |
| AlO <sub>3</sub>                         | aluminum oxide                                     |
| $\alpha$ -Al <sub>2</sub> O <sub>3</sub> | alpha-phase aluminum oxide, also known as corundum |
| cm <sup>-1</sup>                         | reverse centimeter                                 |
| CTE                                      | coefficient of thermal expansion                   |
| DAQ                                      | data acquisition                                   |
| Er                                       | erbium   |
| FTIR                                     | Fourier transform infrared                         |
| InGaAs                                   | indium gallium arsenide                            |
| LHP                                      | laser heated pedestal growth                       |
| LNT                                      | liquid nitrogen temperature                        |
| MBE                                      | molecular beam epitaxy                             |
| MgO                                      | magnesium oxide                                    |
| N  | refractive index                                   |
| NiO                                      | nickel oxide                                       |
| O  | oxygen   |
| OPO                                      | optical parametric oscillator                      |
| RE                                       | rare earth   |
| RT                                       | room temperature                                   |
| Si                                       | silicon  |
| SiO <sub>2</sub>                         | silicon oxide                                      |
| SPS                                      | spark plasma sintering                             |

|                               |                                |
|-------------------------------|--------------------------------|
| SSCC                          | solid-state crystal conversion |
| XRD                           | x-ray diffraction              |
| Y <sub>2</sub> O <sub>3</sub> | yttrium oxide                  |
| YAG                           | yttrium aluminum garnet        |
| YAlO <sub>3</sub>             | yttrium aluminum oxide or YAP  |
| Yb                            | ytterbium                      |

| NO. OF<br>COPIES | ORGANIZATION   |
|------------------|--|
| 1<br>ELEC        | ADMNSTR<br>DEFNS TECHL INFO CTR<br>ATTN DTIC OCP<br>8725 JOHN J KINGMAN RD STE 0944<br>FT BELVOIR VA 22060-6218  |
| 1                | US ARMY RSRCH DEV AND ENGRG CMND<br>ARMAMENT RSRCH DEV & ENGRG CTR<br>ARMAMENT ENGRG & TECHNLOGY CTR<br>ATTN AMSRD AAR AEF T J MATTS<br>BLDG 305<br>ABERDEEN PROVING GROUND MD 21005-5001  |
| 1                | US ARMY INFO SYS ENGRG CMND<br>ATTN AMSEL IE TD A RIVERA<br>FT HUACHUCA AZ 85613-5300  |
| 1                | US GOVERNMENT PRINT OFF<br>DEPOSITORY RECEIVING SECTION<br>ATTN MAIL STOP IDAD J TATE<br>732 NORTH CAPITOL ST NW<br>WASHINGTON DC 20402  |
| 9                | US ARMY RSRCH LAB<br>ATTN RDRL WMM E A SUTORIK<br>ATTN RDRL WMM E G A GILDE (4 COPIES)<br>ATTN RDRL WMM E R PAVLACKA (4 COPIES)<br>BLDG 4600<br>ABERDEEN PROVING GROUND MD 21005   |
| 19               | US ARMY RSRCH LAB<br>ATTN IMAL HRA MAIL & RECORDS MGMT<br>ATTN RDRL CIO LL TECHL LIB<br>ATTN RDRL CIO LT TECHL PUB<br>ATTN RDRL SEE M G NEWBURGH<br>ATTN RDRL SEE M J ZHANG<br>ATTN RDRL SEE M L MERKLE<br>ATTN RDRL SEE M M DUBINSKIY (4 COPIES)<br>ATTN RDRL SEE M N TER-GABRIELIAN<br>ATTN RDRL SEE M T SANAMYAN (6 COPIES)<br>ATTN RDRL SEE M V FROMZEL<br>ATTN RDRL SEE M Z FLEISCHMAN<br>ADELPHI MD 20783-1197 |
| TOTAL:           | 32 (31 HCS, 1 ELEC)  |

INTENTIONALLY LEFT BLANK.